Supporting Information: Real-time Mechanistic Study of Carbon Nanotube Anion Functionalisation through Open Circuit Voltammetry

Adam J. Clancy,[a,b] Pichamon Sirisinudomkit,[b,c] David B. Anthony,[b] Aaron Z. Thong,[c] Jake L. Greenfield,[b] Maniesha K. Salaken Singh,[b] Milo S. P. Shaffer*[b,c]

a) Department of Chemistry, University College London, WC1E 7JE, UK
b) Department of Chemistry, Imperial College London, SW7 2AZ, UK
c) Department of Materials, Imperial College London, SW7 2AZ, UK

AUTHOR INFORMATION

Corresponding Author Email: m.shaffer@imperial.ac.uk

Contents

1. Single-Walled Carbon Nanotubes Density of States

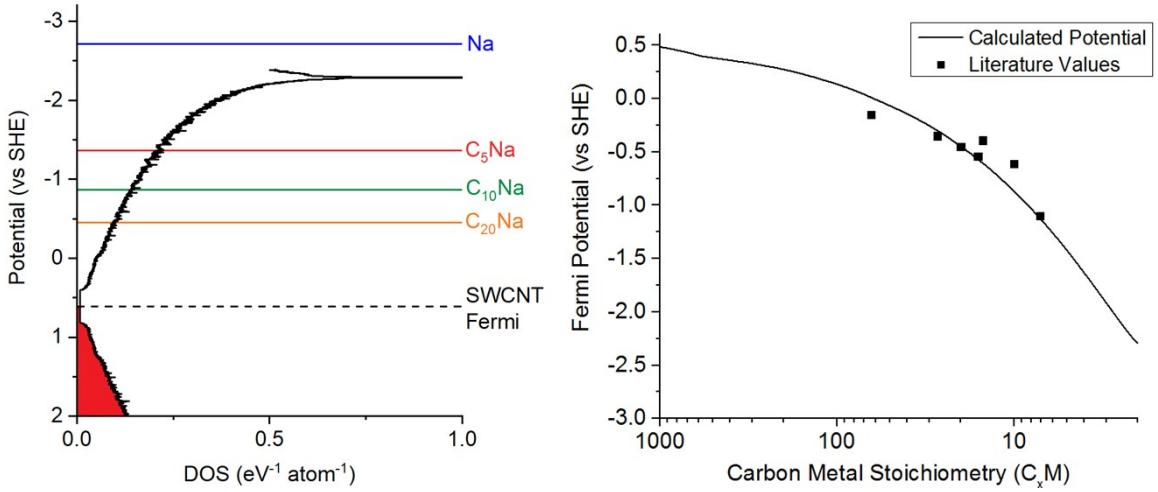

Figure S1. Averaged density of states of all single walled carbon nanotubes (SWCNTs) with diameters between 1 to 2 nm. Left, DOS overlaid with exemplar calculated Fermi levels of C_5M, $C_{10}M$ and $C_{20}M$ and reduction potential of sodium metal. Right, semi-log plot of calculated Fermi level as a function of reducing metal stoichiometry (from integration of DOS, left), with literature values (Table S1).

A universal, chirality independent nanotube Fermi energy of 0.61 eV is taken from converting the SWCNT bundle work function[1] of 5.05 V to the absolute electrode potential ($E_{abs} = E_{SHE} + 4.44$ V). A range of values for Fermi level are available in the literature; whilst the reasons for the discrepancies are not entirely clear, the general trends in the current study do not rely on the precise value.[2] Individual densities of states were downloaded from the website of Prof Shigeo Maruyama, University of Tokyo, (www.photon.t.u-tokyo.ac.jp/~maruyama/kataura/kataura.html) and an average of all helicities from 1-2 nm was taken. Assuming full charge transfer from metal to nanotube, the electron density between neutral SWCNT Fermi level and nanotubide Fermi level is assumed to equal the metal stoichiometry (e.g. 0.05 for $C_{20}M$), allowing the potential of the charged species to be calculated.

While this simple method ignores electron-electron repulsion and quantum capacitance (which may be expected to raise the reduction potentials of the nanotubides through 'stretching' of the density of states[3]), and chirality distribution of a real sample, the results are comparable to experimentally measured values (Table S1).

Table S1. Density of states and reduction potential (E°) verses standard hydrogen electrode (SHE).

Stoichiometry	Change from neutral CNT (V)	Calculated E° vs SHE (V)	Literature Values (V)
C	0	+0.61	
$C_{64}M$	0.59	+0.02	-0.15 [4]
$C_{27}M$	0.90	-0.29	-0.35 [4]
$C_{20}M$	1.06	-0.45	-0.45 [4]
$C_{16}M$	1.17	-0.56	-0.54 [4]
$C_{15}M$	1.21	-0.60	-0.39 [5]
$C_{10}M$	1.48	-0.87	-0.61 [4]
$C_{7.14}M$	1.73	-1.12	-1.10 [6]
C_5M	2.04	-1.43	

[4]) K-doped SWCNT where undoped SWCNT was at +0.57 V

[5]) "For the sample with C/K=15 (0.066 e^- /C) we observe ΔE_F=1 eV". Fermi level difference applied to +0.61 V vs SHE used as the baseline in the current model.

[6]) ~0.14 eq. intercalated K in HiPCO SWCNT bundle

2. Experimental Procedures

2.2 Materials

Tuball SWCNTs (75%, Batch 4-18032014) were purchased from OCSiAl (RUS). 1-Bromopentane (98%), 2-bromo-2-methylbutane (95%), 3-methylbenzyl bromide (96%), 4-(trifluoromethyl)benzyl bromide (98%), 4-(methylthio)benzyl bromide (97%), acetonitrile (99.8%, anhydrous) N,N-dimethylacetamide (99.8% anhydrous, DMAc), N,N-dimethylformamide (99.8% anhydrous, DMF), naphthalene (99%), silver nitrate (99.999%), phosphorous pentoxide (≥98.0%), sodium (99.95% ingot), sodium dodecyl sulfate (≥99.0 %), and tetrabutylammonium perchlorate (≥99.0 %) were purchased from Sigma-Aldrich Ltd. (GBR). 2-Bromopentane (90 %), 3-(trifluoromethyl)benzyl bromide (98%), 4-nitrobenzyl bromide (99%), ethanol (absolute ≥99.8%), and acetone (≥99%) were purchased from VWR Ltd. (GBR). 3-Methoxybenzyl bromide (98%) and 4-methylbenzyl bromide (98%) were purchased from Fischer Scientific Ltd. (USA), 3-nitrobenzyl bromide (95%) was purchased from Fluorochem Ltd. (GBR), and sodium perchlorate (98.0-102.0% anhydrous) was purchased from Alfa Aesar (USA).

Chemicals were used without further purification bar 2-bromopentane (distilled under vacuum) and SWCNTs (*vide infra*). The liquid alkyl halides were degassed via freeze-pump-thaw before transferring to the glovebox, and dried over activated 3 Å molecular sieves for two days before use. DMAc, DMF, and acetonitrile were transferred directly to the glovebox and dried with activated 3 Å molecular sieves for two days before use. Naphthalene and tetrabutylammonium perchlorate, were dried in a vacuum oven (ca. 50 mbar, 50 °C) in the presence of P_2O_5 for 16 h before placing under vacuum and transferring to the glovebox.

2.3 Synthesis and Procedures

All work involving sodium naphthalide (NaNp) and/or reduced SWCNTs was performed in an mBraun glovebox (nitrogen atmosphere, < 0.1 ppm water, < 0.1 ppm oxygen). All glassware, including glass stirrer bars, were dried before use (140 °C, 1 h minimum).

2.3.1 Sodium Naphthalide

NaNp/DMAc solution was prepared by stirring equimolar sodium and naphthalene in dry solvent using a glass coated stirring bar until all sodium dissolved (~1 h). Solution quantities varied from 10 mL to 1000 mL and concentrations kept below 0.15 mM. Solutions were kept sealed and out of direct sunlight when not in use and were used within a week of synthesis.

2.3.2 SWCNT Purification

The procedure to accelerate large scale purification of SWCNTs was adapted from Clancy et al.[7] and is shown in Fig. S2. Raw Tuball SWCNT powder (1.51 g) was dried under vacuum at 250 °C for 2 h before transferring to a glovebox. The SWCNTs were placed in a Pyrex cafetière à piston, (Genware, 1 L, 8-cup) without the mesh plunger inserted. Pre-prepared NaNp solution (290 mg Na, 1.61 g $C_{10}H_8$, 750 mL DMAc, 10:1 SWCNT:Na) was poured over the SWCNTs and left for 48 h, after which the plunger is inserted and slowly depressed. The solution of SWCNT impurities was decanted to leave the purified SWCNTs behind. The residual nanotubes were exposed to a dry O_2/N_2 (20:80) atmosphere for 20 min before washing with ethanol, water and acetone, using the cafetière to separate washings to give purified SWCNTs (1.1 g, 73% mass yield).

Figure S2. Pictures of cafetière assisted SWCNT purification. (a) Raw SWCNT powder, (b) NaNp/DMAc solution added to SWCNT powder immediately causing pitch black solution to form. (c) After 48 h, mixture has become a gel, with surface of mixture clearly uneven. (d) Impurities may be poured off to leave purified SWCNTs in the cafitiere.

2.3.3 *Nanotubide Functionalization*

Pre-prepared sodium naphthalide solution (1.92 mg(Na)) was diluted to 20 mL with DMAc, and poured over purified SWCNTs (10 mg) and stirred overnight with a glass stirrer bar to give nanotubide solution. The nanotubes were functionalized through addition of alkyl halide (0.25 mmol, 3 eq. vs Na) and stirred overnight. The SWCNTs were then discharged with bubbling of dry O_2/N_2 (20:80), and filtered over a polytetrafluoroethylene (PTFE) membrane (100 nm pore size) and washed with copious ethanol, water and acetone to give the functionalized SWCNTs.

2.3.4 *SWCNT Buckypaper Synthesis*

Sodium dodecyl benzenesulfonate (0.5 g) was stirred in deionized water (50 mL) overnight. Purified Tuball SWCNTs (50 mg) were added and the mixture was sonicated with an ultra-sonic processor (Sonic and Materials Inc., 750 W) using a blunt (5 mm) titanium tip for 30 min at 10% power while cooling with an ice bath. The mixture was filtered over a PTFE membrane (100 nm pore size) and washed with copious hot water and ethanol. The buckypaper was dried in a vacuum oven and cut into ca. 10 x 30 mm strips and weighed.

2.3.5 *Open Circuit Voltammetry Measurements*

All electrochemical measurements were performed on Gamry Instruments Interface 1000 potentiostat/galvanostat/ZRA, run with Gamry Instruments Framework™ (v.6.24), with the electrochemical cell in a glovebox using standard electrical feed-throughs. All experiments were performed in a custom 4-necked quartz cell. The reference and counter electrodes were silver and platinum wires respectively, sonicated in absolute ethanol for 30 min and dried at 400 °C, and placed in glass enclosure with an ion permeable glass frit at the bottom. The frits were soaked in acetonitrile and dimethylformamide respectively for two days before use. The enclosures were filled by $AgNO_3$ (0.01 M in MeCN, reference) and tetrabutylammonium perchlorate (0.1 M in DMF, counter electrode) solution, each dried over 3 Å molecular sieves for 1 day after mixing. A preweighed SWCNT buckypaper attached to a copper clip on a platinum wire was used for the working electrode. The electrode was submerged to ensure the full buckypaper was beneath the electrolyte; due to the significantly higher surface area of the SWCNTs, the contribution of the copper, under the strongly reducing conditions applied, was ignored. Open circuit voltammetry (OCV) was measured with 1 s resolution. For addition of sodium naphthalide solution, 0.1 eq. sodium vs SWCNT (assuming Mw = 12) was added from above and allowed to diffuse into solution. For addition of organic species, 3 molar eq. versus SWCNT buckypaper was added from above. First derivatives of OCV with regards to time were smoothed with 50pt Savitzky-Golay in *OriginPro 2018*.

2.4 Characterization

2.4.1 Thermogravimetric Analysis

Thermogravimetric analysis (TGA) were run on a Mettler Toledo TGA/DSC1 with lidded 70 µL alumina pans, manually removing a premeasured background. TGAs were carried out on ca. 1 mg of material with a gas flow rate of 60 sccm. The samples were heated from 30 to 100 °C at 45 °C min^{-1} before holding for 30 min (to remove residual water and sparge the furnace) before heating at 10 °C min^{-1} to 850 °C. For the calculation of grafting density of functionalized materials, the percentage weight loss was taken at 530 °C minus the weight loss of the unfunctionalized SWCNTs. Grafting densities (R/C) are given as the molar ratio of reacted material (Mw = Initial Mw – 79.9 to account for Br loss) and SWCNT (Mw = 12).

2.4.2 Cyclic Voltammetry Measurements

For cyclic voltammetry, sodium perchlorate (7 mL, 50 mM, DMF) was used as the electrolyte with 1 mM of organobromide. Samples were held at the OCV for 30 s to remove any residual charge from the electrodes before cycling between +0.1 and -1.0 V to settle the system and form a stable double layer. The potential was then cycled between +0.1 and -2.4 V vs $Ag/AgNO_3$ at 50 mV s^{-1} twice to ensure the reproducibility of the CV (only first curve provided, which typically shows better signal due to degradation of organobromides after the first cycle). Reduction potentials were measured at the nadir of dI/dV derivatives.

2.4.3 Raman Spectroscopy

Raman spectroscopy was performed on a Renishaw InVia micro-Raman Spectrometer using a 532 nm (32 mW) laser with 1800 nm grating, centered around 1450 cm^{-1} over a >200 μm^2 region for >1500 measurements. Fitting for D/G mode ratios was performed using *WiRE 4.1*, after background ('intelligent fitting', 11th order polynomial, 1.50 noise tolerance) followed by peak-fitting D (1340 cm^{-1}) and G (1589 cm^{-1}) modes. Values given as intensity ratios.

3. Supplementary Open Circuit Voltammetry

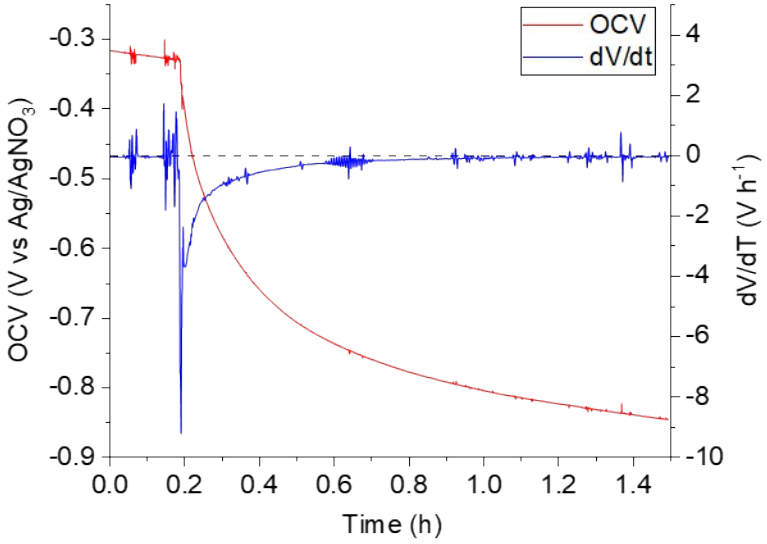

Figure S3. Open circuit voltammetry (and derivative) of buckypaper working electrode with addition of NaNp. NaNp was added after 10 min (0.167 h) showing that the majority of charge change occurs within 1 h, with OCV drift virtually returning to initial (pre-NaNp) drift after this point (minor negative drift is seen 24 h after NaNp addition). Dashed line represents dV/dt = 0.

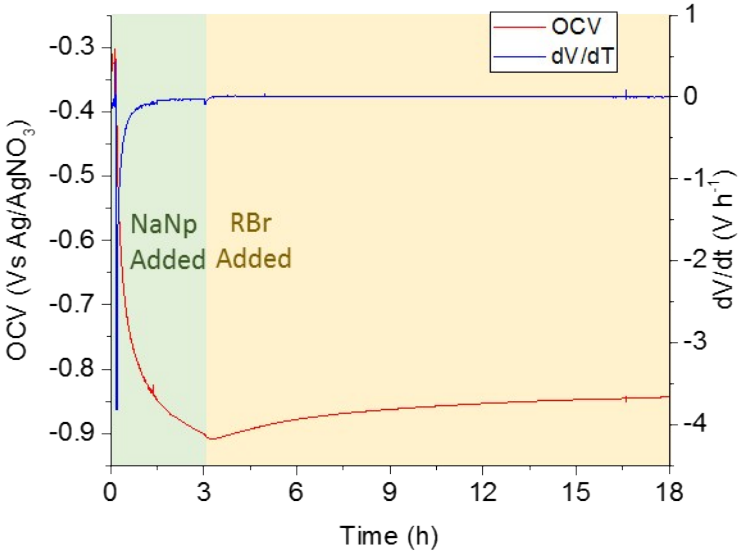

Figure S4. Figure 2 from main text showing full derivative range. OCV and dV/dt during sodium naphthalide reduction at 15 min, and bromobutane addition 195 min.

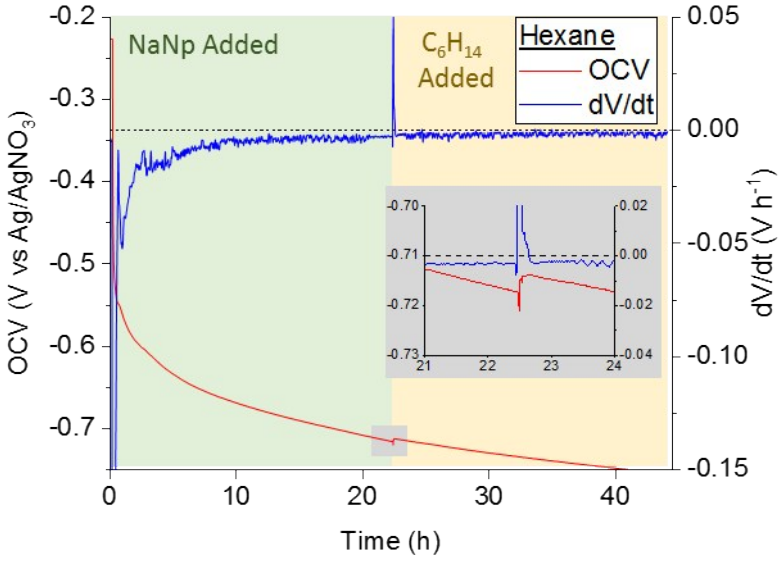

Figure S5. Open circuit voltammetry (and derivative) versus time of buckypaper working electrode after addition of sodium naphthalide solution, with addition of n-hexane 22 h after NaNp addition. Dashed line represents dV/dt = 0. Inset shows zoomed region over 3 h around point of organic addition, highlighted in the main plot. The +0.003 V OCV offset upon hexane addition is followed by the OCV continuing at the same rate as prior to hexane addition. The offset is attributed to a small decrease in the stability of sodium cations in solution due to the addition of non-polar hexane, leading to a small increase in proportion of associated cations on the nanotubide surface.

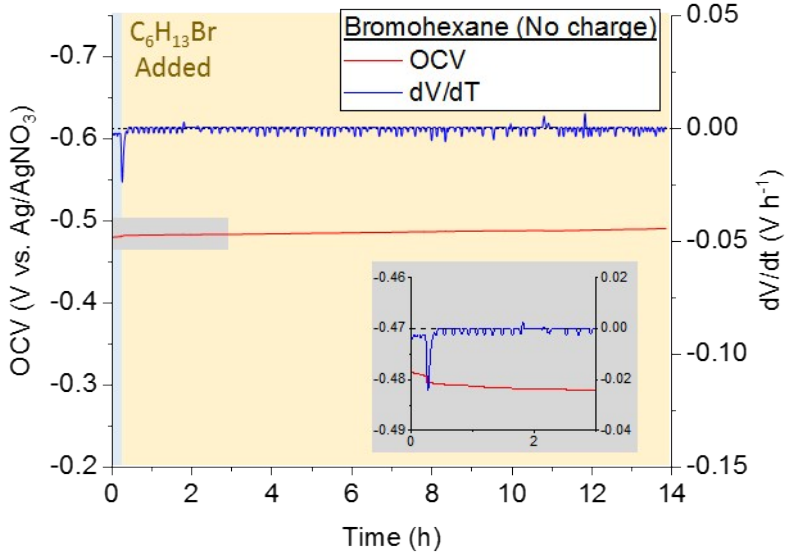

Figure S6. Open circuit voltammetry (and derivative) versus time of buckypaper working electrode at rest (blue background) and during addition of 1-bromohexane (0.25 h, yellow background). Dashed line represents dV/dt = 0. Inset shows zoomed region over 3 h around point of organic addition, highlighted in the main plot. The dip in potential on bromohexane addition lasted 1 data point (1 s resolution) in contrast to the >10 minutes seen for reduced SWCNTs and organohalide (Fig S7 and Fig 2 main text) and is attributed to physical instability from the motion of adding the liquid.

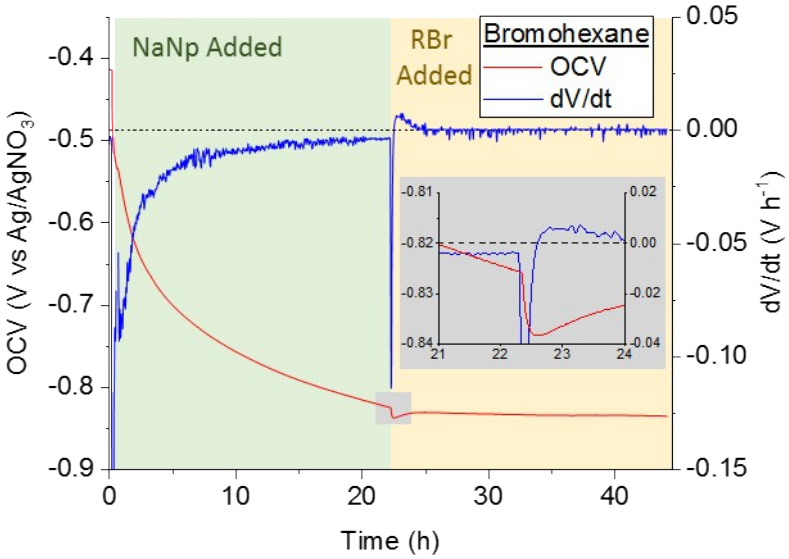

Figure S7. Open circuit voltammetry (and derivative) versus time of buckypaper working electrode after addition of sodium naphthalide solution, with addition of 1-bromohexane 22 h after NaNp addition. Dashed line represents dV/dt = 0. Inset shows zoomed region over 3 h around point of organic addition, highlighted in the main plot. Data between 1.51 to 1.93 h removed due to noise from environmental effects.

4. Computational Methods

Bond dissociation (Δ_{EBDE}) and heterolytic bond cleavage (ΔE_{Het}) energies were calculated using the *ab initio* Gaussian-3 (G3) method, geometries determined by second order Moller-Plesset perturbation theory (MP2), using B3LYP structures/frequencies. While DFT is more common for heterolytic bond cleavage calculations, it is not appropriate for radical energies,[8] so G3MP2B3 was used for all calculations for consistency. ΔE_{Het} and ΔE_{BDE} are given as the summed ground state energies of the organic cation/radical and bromide/bromine minus the energy of the parent organobromide. Input atomic coordinates were obtained from MM2 force field relaxation in *ChemBio3D Ultra (v.14.0.0.117)*. All obvious conformations for benzyl compounds were relaxed via MM2 and the lowest total energy geometry was used as G3MP2B3 input coordinates. Default geometric optimisation in *Gaussian* was performed prior to G3MP2B3 calculation.

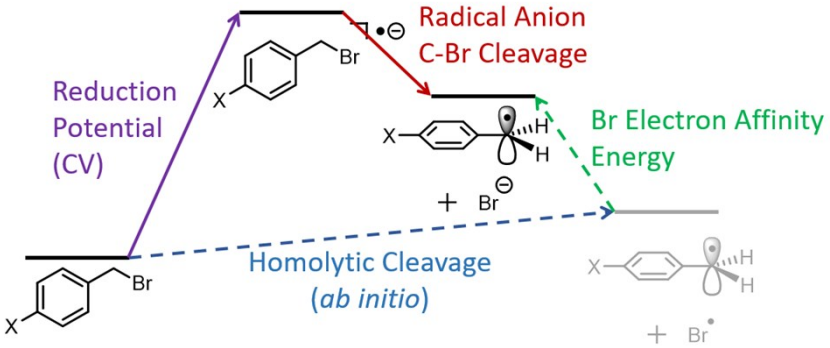

Figure S8. Schematic Hess cycle for RBr intermediates proposed in SET mechanism (Main text, Fig. 1), with indications of how each intermediate was probed. Notably, $XPhCH_2^{\bullet}$ + Br^- is never directly probed, but the enthalpy change from the parent $XPhCH_2Br$ may be calculated from homolytic cleavage of C-Br offset by Br electron affinity.

5. Supplementary Thermogravimetric Analysis Thermograms

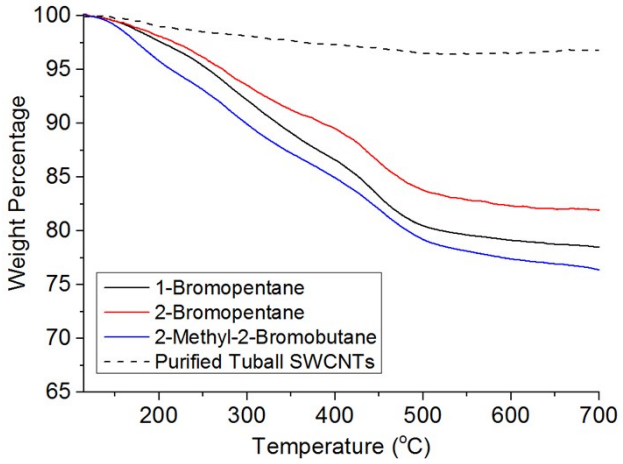

Figure S9. TGA thermograms from functionalization of SWCNTs reductively functionalized with bromohexane isomers.

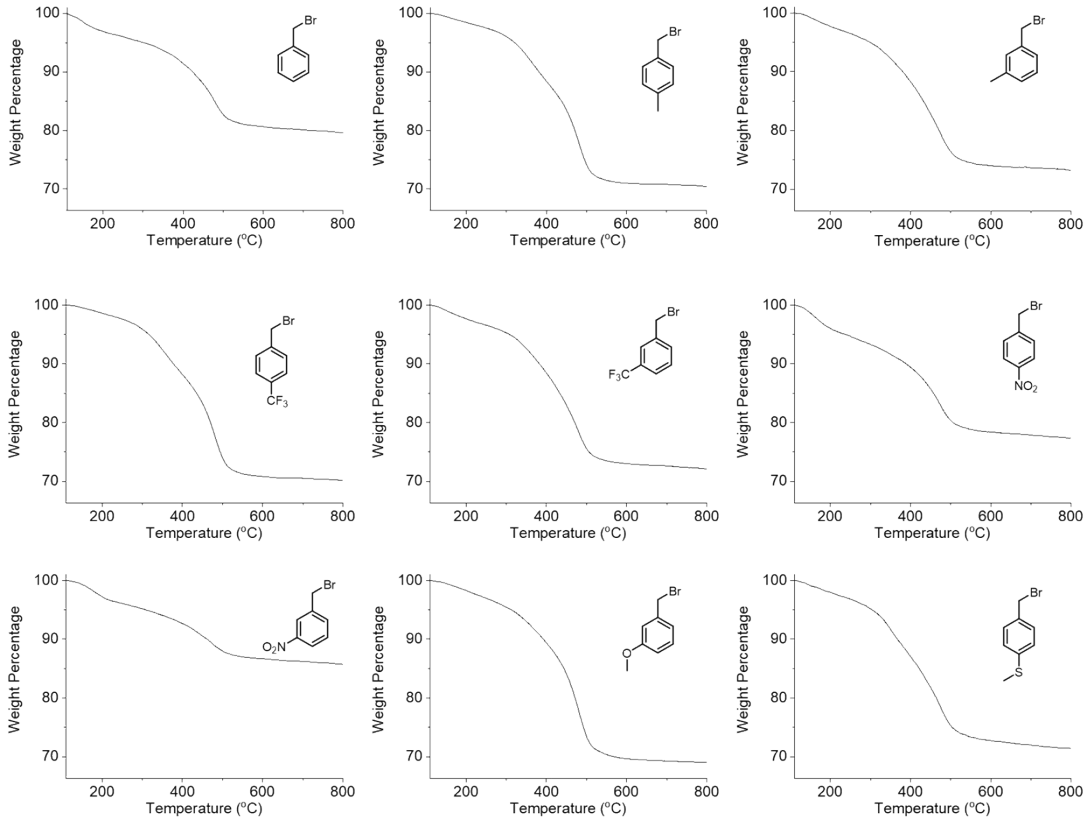

Figure S10. TGA thermograms of SWCNTs functionalized with benzyl bromides.

6. Cyclic Voltammograms of Benzyl Bromides

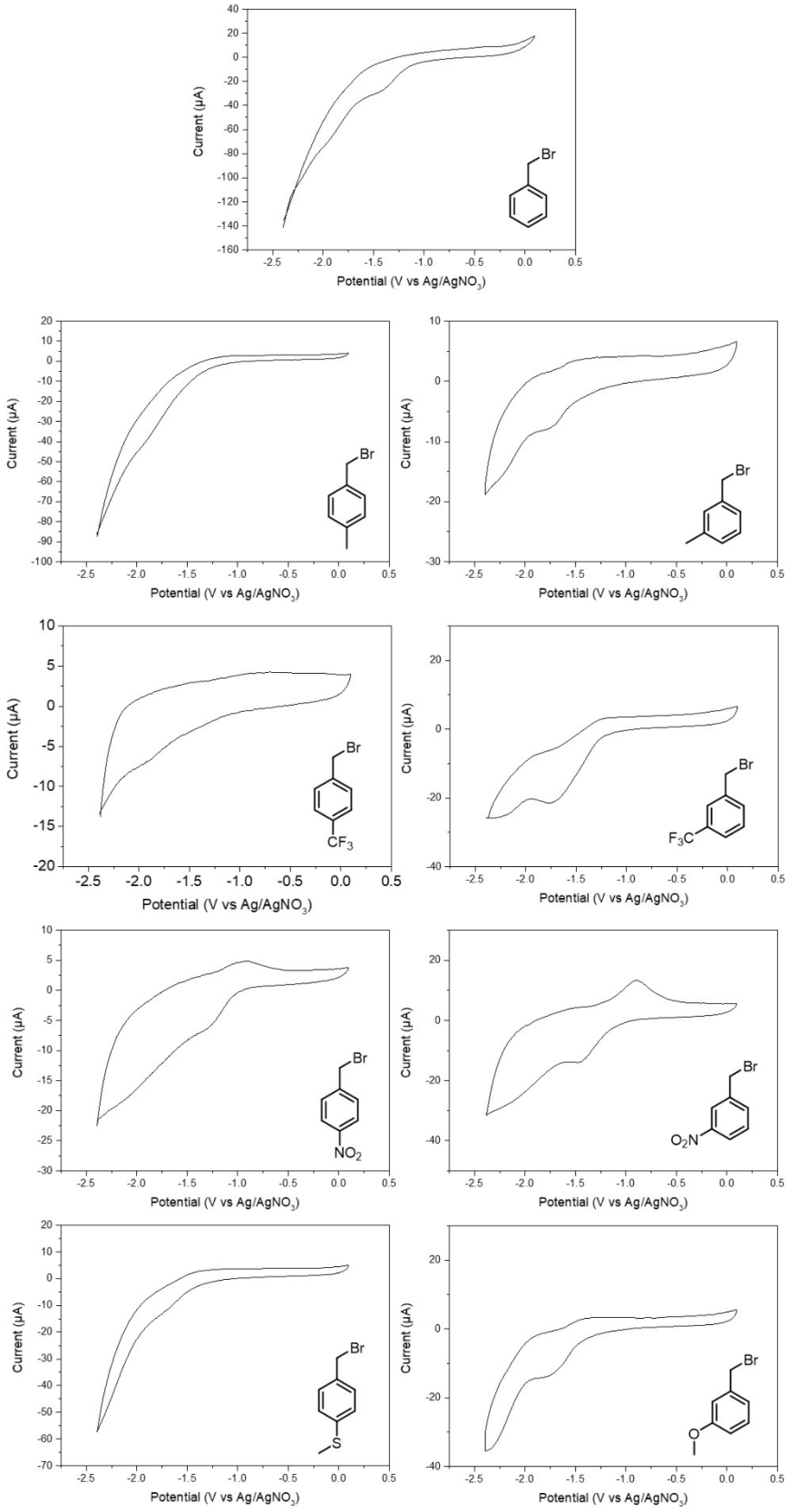

Figure S11. Cyclic voltammograms of benzyl bromides.

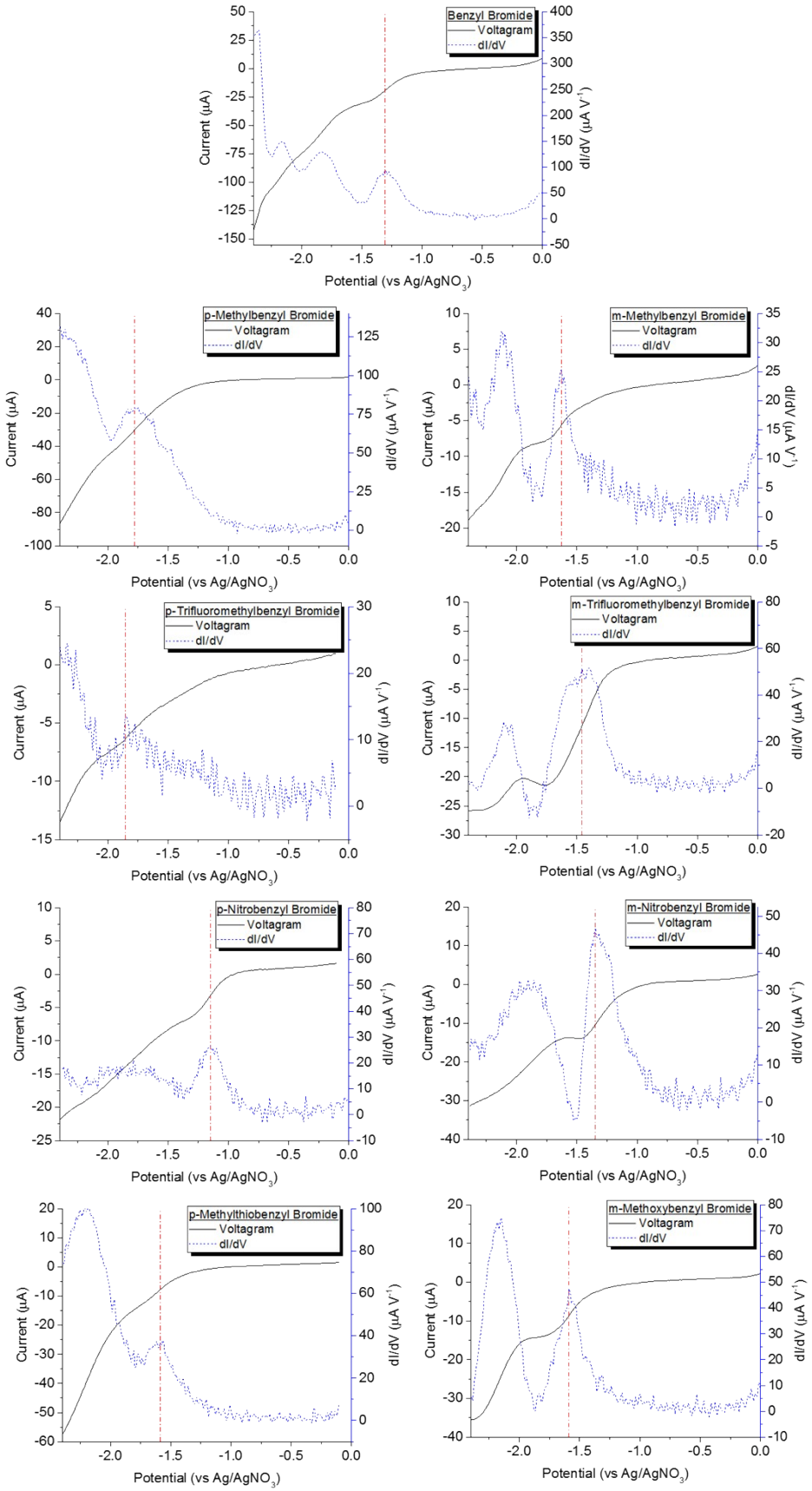

Figure S12. First reductive sweep of CV (black solid) with dI/dV (blue dotted) and derivative peak used for reduction trends (red dashed)

7. Raman Data of Benzyl Bromide Functionalized SWCNTs

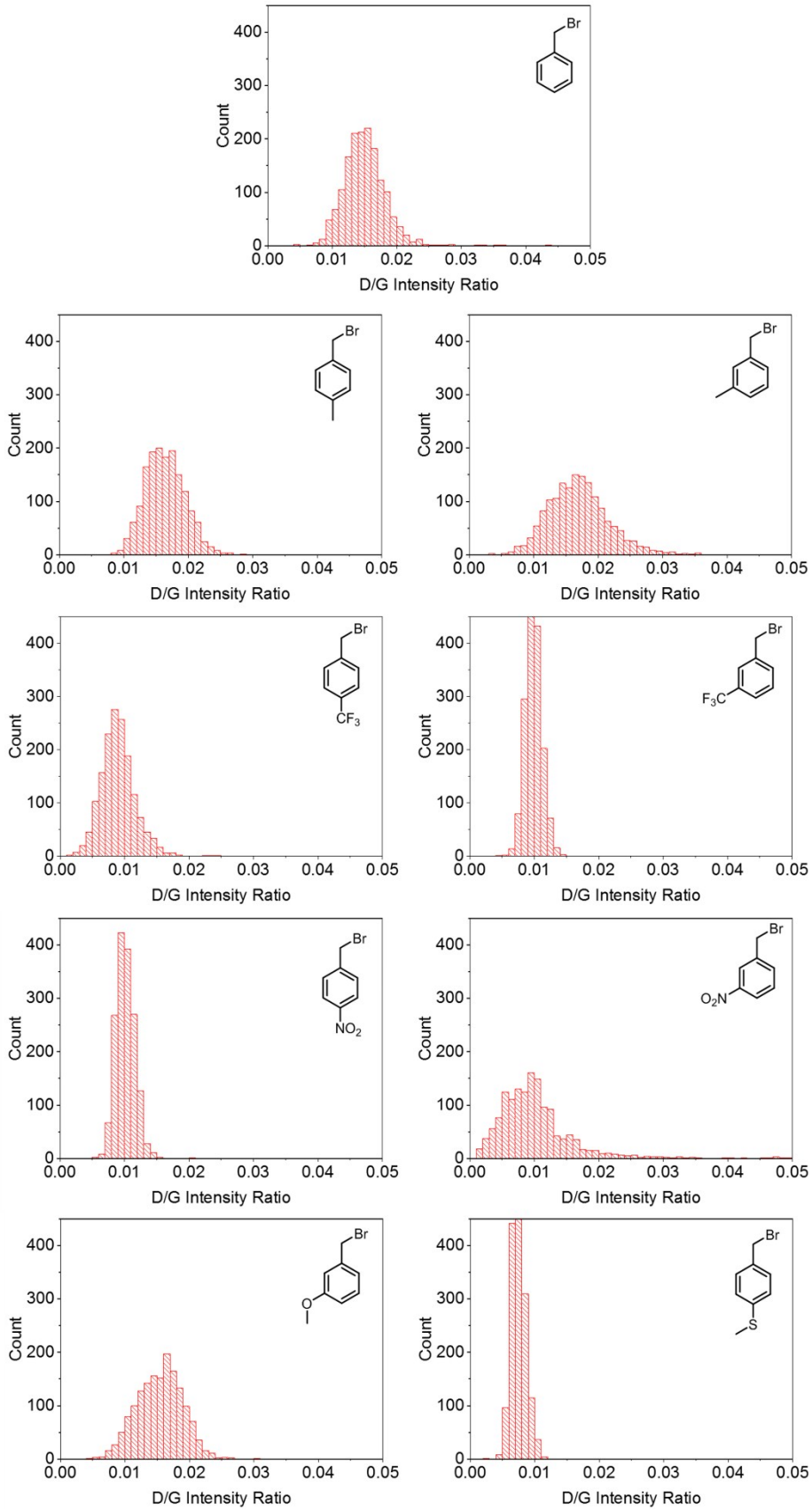

Figure S13. Statistical Raman D/G mode intensity ratios (N = 1656 – 1872) of benzyl bromide functionalized SWCNTs (bin size 0.0125; 40 bins over D/G 0 – 0.5)

8. Tabulated Benzyl Bromide Data

Table S2. SWCNTs and monosubstituted benzyl bromides reaction data and benzyl bromides properties. Grafting density (C/R) quantified by TGA, Raman spectra intensity D-mode/intensity G-mode ratio. Hammett parameters taken from Hansch,[9] calculated heterolytic bond dissociation energy (ΔH_{BDE}) and homolytic bond cleavage energy (ΔH_{Het}), and cyclic voltammetry (CV) determined reduction potential (E°). Bottom rows show Pearson correlation coefficient (R^2) of each variable versus grafting density and two-tailed significance (p)

$BrCH_2PhR$		**TGA**	**Raman**	**Hammet**	**ΔE_{cleave}[RBzBr]**		**CV**
R	para/meta	R/C	D/G	σ	ΔH_{Het} (kJ mol^{-1})	ΔH_{BDE} (kJ mol^{-1})	E° (V vs $Ag/AgNO_3$)
H	-	0.03401	0.01494	0.00	617.247	535.071	-1.673
Me	Para	0.04878	0.01640	-0.17	587.771	529.526	-1.512
Me	Meta	0.04386	0.01694	-0.07	608.050	548.608	-1.380
OMe	Meta	0.04484	0.01544	0.12	605.419	549.411	-1.481
SMe	Para	0.03571	0.00750	0.00	549.042	545.665	-1.935
CF_3	Para	0.02457	0.00893	0.54	658.496	528.234	-1.919
CF_3	Meta	0.02227	0.01023	0.43	656.330	529.494	-2.010
NO_2	Para	0.02591	0.01017	0.78	676.442	532.608	-2.095
NO_2	Meta	0.01473	0.01013	0.71	673.241	536.357	-1.885
		R^2 (vs R/C)		0.871	0.765	0.474	0.812
		p (vs R/C)		0.0023	0.0164	0.1677	0.0078

9. References

1. Shiraishi, M.; Ata, M. Work Function of Carbon Nanotubes. *Carbon* **2001,** *39* (12), 1913-1917.
2. Hodge, S. A.; Bayazit, M. K.; Coleman, K. S.; Shaffer, M. S. Unweaving the Rainbow: A Review of the Relationship Between Single-Walled Carbon Nanotube Molecular Structures and Their Chemical Reactivity. *Chem. Soc. Rev.* **2012,** *41* (12), 4409-4429.
3. Hodge, S. A.; Tay, H. H.; Anthony, D. B.; Menzel, R.; Buckley, D. J.; Cullen, P. L.; Skipper, N. T.; Howard, C. A.; Shaffer, M. S. Probing the Charging Mechanisms of Carbon Nanomaterial Polyelectrolytes. *Farad. Discus.* **2014,** *172*, 311-325.
4. Zhao, J.; Han, J.; Lu, J. P. Work Functions of Pristine and Alkali-Metal Intercalated Carbon Nanotubes and Bundles. *Phys. Rev. B* **2002,** *65* (19), 193401.
5. Pichler, T.; Rauf, H.; Knupfer, M.; Fink, J.; Kataura, H. In *A Photoemission Study of Potassium-Doped Single Wall Carbon Nanotubes*, AIP Conf. Proc., 2004; AIP, pp 217-221.
6. Suzuki, S.; Maeda, F.; Watanabe, Y.; Ogino, T. Electronic Structure of Single-Walled Carbon Nanotubes Encapsulating Potassium. *Phys. Rev. B* **2003,** *67* (11), 115418.
7. Clancy, A. J.; White, E. R.; Tay, H.; Yau, H.; Shaffer, M. Systematic Comparison of Conventional and Reductive Single-Walled Carbon Nanotube Purifications. *Carbon* **2016,** *108*, 423-432.
8. Izgorodina, E. I.; Brittain, D. R.; Hodgson, J. L.; Krenske, E. H.; Lin, C. Y.; Namazian, M.; Coote, M. L. Should Contemporary Density Functional Theory Methods Be Used to Study the Thermodynamics of Radical Reactions? *J. Phys. Chem. A* **2007,** *111* (42), 10754-10768.
9. Hansch, C.; Leo, A.; Taft, R. A Survey of Hammett Substituent Constants and Resonance and Field Parameters. *Chem. Rev.* **1991,** *91* (2), 165-195.